Forest Water Use is Increasingly Decoupled from Water Availability Even During Severe Drought

Katie A. McQuillan (✉ kmcquil@ncsu.edu)

North Carolina State University at Raleigh: NC State University   https://orcid.org/0000-0001-7302-719X

Mirela G. Tulbure

North Carolina State University at Raleigh: NC State University

Katherine L. Martin

North Carolina State University at Raleigh: NC State University

Abstract

Context: Key to understanding forest water balances is the role of tree species regulating evapotranspiration (ET), but the synergistic impact of forest species composition, topography, and water availability on ET and how this shapes drought sensitivity across the landscape remains unclear.

Objectives: Our aims were to quantify (1) the effect of forest composition and topography including elevation and hillslope gradients on the relationship between ET and water availability, and (2) whether the relationship has changed over time.

Methods: We used remotely sensed Landsat and MODIS ET to quantify forest ET across the Blue Ridge ecoregion of the southeastern USA. Then quantified metrics describing ET responses to water availability and trends in responses over time and assessed how these metrics varied across elevation, hillslope, and forest composition gradients.

Results: We demonstrated forest ET is becoming less constrained by water availability at the expense of lateral flow. Drought impacts on ET diverged along elevation and hillslope gradients, and that divergence was more pronounced with increasingly severe drought, indicating high elevation and drier, upslope regions tend to maintain ET rates even during extreme drought. We identified a decoupling of ET from water availability over time, and found this process was accelerated at higher elevations and in areas with more diffuse-porous trees.

Conclusions: Given the large proportion of forests on the landscape distributed across high elevation and upslope positions, reductions in downslope water availability could be widespread, amplifying vulnerability of runoff, the health of downslope vegetation, and aquatic biodiversity.

1. Introduction

Forest water cycles are accelerating in response to changing climate, which could stress water resources, even in humid, traditionally water-rich ecoregions. The stable supply of forest water-based ecosystem services is essential to the continued support of the diverse aquatic ecosystems as well as downstream supplies for drinking water, agriculture, and energy. Forest evapotranspiration (ET) is the flux of water returned rapidly to the atmosphere, and partitioning of water to ET determines downstream water availability (Fisher et al., 2017). Precipitation entering a watershed is either partitioned towards ET, or it continues in the water cycle as runoff or groundwater available downslope for plants or streams (Falkenmark & Rockström, 2006). Changes in ET relative to precipitation drive changes in local water availability, and when such shifts happen over large portions of a watershed, they cause alterations in streamflow (Caldwell et al., 2016; Orth & Destouni, 2018; Teuling et al., 2013). A ten percent increase in ET has been observed globally from 2003 to 2019, and has been attributed to rising temperatures, increasing evaporative demand, longer growing seasons, and changing forest tree species composition (Caldwell et al., 2016; Hwang et al., 2018; Pascolini-Campbell, Reager, Chandanpurkar, & Rodell, 2021). Given increasing water demand from forests and the potential for less water in our rivers in the future, it is

important to understand the control forests exert on water availability across landscapes and over time, especially during periods of water stress (Fisher et al., 2017).

In complex topography, forest ET response to water stress at one part of the landscape can directly affect water availability at other, connected parts of the landscape, as well as streamflow (Bales et al., 2018). Therefore, it is critical to understand the feedbacks between vegetation and topography to quantify landscape forest hydrology. Two major components of topographic complexity, elevation and hillslope gradients, control the abiotic conditions and create microclimates that influence vegetation characteristics (Fan et al., 2019). Elevation gradients contribute to systematic changes in vegetation species composition, temperature regimes, and can moderate or accelerate global change (Kelly & Goulden, 2008; Rangwala & Miller, 2012). Hillslope gradients describing ridge to valley convergence control lateral flow (Fan et al., 2019). Soil moisture is organized along hillslope gradients following lateral flow with higher soil moisture found in valleys and lower soil moisture found upslope (Tromp-van Meerveld & McDonnell, 2006).

Topographic patterns in water availability and microclimate shape landscape vegetation patterns, with increasing LAI and biomass supported by wetter downslope positions compared to drier upslope positions (Hwang, Band, Vose, & Tague, 2012; Hwang et al., 2020; Tai et al., 2020). Further, downslope positions are characterized by tree species that tend to use more water and are more sensitive to drought (Lin et al. 2019). In the southern Appalachians, mesic species trees with diffuse-porous xylem, including maples (*Acer* sp) and tulip-poplars (*Liriodendron tulipifera*) are over two times as sensitive to soil drying and can transpire up to four times the amount of water as similar sized xeric species with ring-porous xylem, like oaks (*Quercus* sp.) and hickories (*Carya* sp.) (Ford, C. R., Hubbard, R. M., & Vose, J. M, 2011). While diffuse-porous species have historically been associated with downslope, wetter positions, humid forests of the eastern US have undergone a process called "mesophication." A history of fire suppression, in addition to shifts in precipitation and temperature distributions, has led to a shift in dominance from disturbance tolerant xeric species to shade tolerant mesic species (Nowacki & Abrams, 2008; Pederson et al., 2015). Mesic species are now found throughout the landscape, increasing ET and decreasing downstream runoff (Elliott & Swank, 2008; Elliott, Miniat, Pederson, & Laseter, 2015). Caldwell et al. (2016) estimated this change in species dominance has increased ET across the southeastern US up to 29% since the mid-1970s.

Whether upslope positions or downslope positions are more drought sensitive is not clear, particularly in the context of changing species composition. Two contrasting mechanisms by which topography could influence forest drought sensitivity have been proposed by Tai (2021). First, topographic convergence in downslope portions of the landscape could buffer ecosystem sensitivity to drought because lateral hydrologic flow down slope would lead to higher water supply. However, convergent areas support higher biomass composed of species with higher daily transpiration rates that are adapted to abundant soil moisture. So, it's also possible that higher water demand of convergent areas could deplete soil moisture more quickly and ultimately result in greater drought sensitivity. A third mechanism, which may overlap with the first two, is also possible. As vegetation capitalizes on lateral flow during drought, it may reduce

downslope water availability and thus increase drought sensitivity at convergent areas (Bales et al., 2018; Hwang et al., 2020). The magnitude of the reduction in downslope water availability and thus, the increase in drought sensitivity downslope, is likely dependent on ET rates and thus, tree species composition.

We investigated the mechanisms of topographic-vegetation drought sensitivity using remote sensing (RS) based ET, allowing us to examine processes at medium resolution across a regional scale. The recent widespread availability of RS based ET provides a novel opportunity to assess forest ET drought responses continuously across space to understand landscape level variation in forest water use over the past two to three decades (Mu, Heinsch, Zhao, & Running, 2007; Senay, Gabriel B., Schauer, Friedrichs, Velpuri, & Singh, 2017; Yang, Y., Anderson, Gao, Hain, & semmens, 2015). To complement RS based ET, gridded standardized drought indices are frequently used to assess spatial patterns of drought severity and their impacts on forests at large spatial scales. Drought indices are often based on water supply (precipitation) and some additionally incorporate water demand (potential evapotranspiration, PET). While indices accounting for both supply and demand are more representative of available water, we focus here on a simple precipitation deficit to facilitate direct comparisons across spatial and temporal scales that could otherwise be influenced by changes in PET.

We investigated the influence of topography and the forest composition on spatial and long term temporal trends of forest water use response to water availability across humid southeastern forests that have undergone mesophication. The impact on forest ET of the expansion of diffuse porous at large scales is not well understood, however, we hypothesized it would interact with topographic gradients, mediating water supply to systematically influence forest water use, and in turn, forest water use would influence subsequent downslope water supply. While there are reports of increasing forest ET and decreasing lateral flow, changes in sensitivity of forest ET to water availability over time and how that relates to local biotic and abiotic conditions is unknown, but could yield large impacts on continued delivery of water-based ecosystem services. Therefore, our aims were to quantify (1) the effect of forest composition and topography including elevation and hillslope gradients on the relationship between ET and water availability, and (2) whether the relationship has changed over time, using multi-sensor RS based ET across the Blue Ridge ecoregion in the southeastern US.

2. Methods

2.1 Study site

2.1.1 General Description

The EPA Level III Blue Ridge ecoregion is approximately 40,940 km^2 and spans parts of the Southern Appalachian Mountains in Virginia, North Carolina, Tennessee, South Carolina, and Georgia (Fig. 1). Elevation ranges from 200 - 2035 m with an average elevation of 764 m. Soils are largely acidic infertile, and categorized as Dystrochrepts and Hapludults. Underlying geology consists mostly of sandstones,

shales, and related rocks that were metamorphosed over to form dominantly steep slopes (Pittillo et al. 1998). Forests are primarily composed of oaks, northern hardwoods, with spruce-fir forests at high elevations. Forest species composition and structure has slowly shifted towards more closed canopy mesic forests over the past 100 years, with increasing abundance of maple and tulip-poplar across the landscape (Elliott & Swank, 2008). While annual rainfall and average temperature varies across elevation and latitudinal gradients, the climate is characterized as warm summer continental with significant precipitation in all seasons. Approximately 75% of the region is forested and increasing development and agricultural land cover is located at lower elevations.

2.1.2 Topographic Gradients

Elevation data was retrieved from the USGS National Elevation Dataset (NED) at ⬚ arc-second (~30m) (Gesch, Evans, Oimoen, & Arundel, 2018) (Fig. S1) and the Topographic Wetness Index (TWI) was calculated using the USGS NED as a function of slope and upslope accumulated area (Beven & Kirkby, 1979). The TWI is representative of water availability fed by lateral drainage and has been frequently used to describe hillslope gradients (Hoylman et al., 2018; Hwang et al., 2012; Tai et al., 2020). Lower TWI values correspond to drier upslope landscape positions and higher TWI values correspond to wetter downslope landscape positions. Elevation and TWI were resampled to match MODIS and Landsat spatial resolution.

2.2 Forest Mapping

2.2.1 Continuous forest cover

We created continuous forest maps and screened out non-forest areas from the analysis at both the MODIS and Landsat scales. The MODIS continuous forest cover map was created using the MODIS Land cover product (MCD12Q1) available from 2001 - 2019 (Friedl & Sulla-Menashe, 2019). We considered pixels classified as forested for all years continuous forest and included them in the analysis. The Landsat continuous forest cover map was created using the NLCD which has classified land cover available for 1992, 2001, 2004, 2006, 2008, 2011, 2013, and 2016 (Yang et al., 2018). Continuous forest cover at Landsat scale using NLCD was mapped following the same procedure as MODIS. All other gridded datasets used in this study were masked to only forest pixels using the relevant MODIS or Landsat continuous forest cover product.

2.2.2 Forest species maps

We used a gridded forest composition dataset to assess forest composition impacts on ET. Riley et al. (2021) developed a 30m tree-level model of the US circa 2014 using machine learning with satellite-derived vegetation, topography, and biophysical grids produced by the LANDFIRE project (landfire.gov, 2017) to assign each forested pixel across the US the Forest Inventory and Analysis (FIA) (fia.fs.fed.us) plot that best represented forest conditions (Riley, Grenfell, Finney, & Wiener, 2021). Model validation

showed that 77% of validation plots matched at least one of the two most frequently occurring tree species in the pixel within the plot diameter, indicating the model seemed to predict tree species with a high level of accuracy. Using the tree-level model, we created a forest composition map characterizing the percent of total basal area (BA) in each cell corresponding to species with diffuse-porous xylem anatomy. The total BA of all species on the landscape was calculated and the 50 most abundant species, accounting for 98.5% of BA, were classified as diffuse-porous, ring-porous, or tracheid (Table S1). Using these classifications, we calculated the percent diffuse-porous BA of total BA for each pixel and then resampled to MODIS and Landsat spatial resolution (Fig. S1). We selected the Riley product because it is higher resolution than other available forest composition products and includes disturbance history in the predictions, which should allow it to better capture the distribution of diffuse-porous species. Additional steps to validate the forest composition map are included in supplementary material.

2.3 Remotely sensed Evapotranspiration

2.3.1 Remotely sensed Evapotranspiration Datasets

Mountainous forested regions have higher uncertainty associated with modeled ET estimates because of the complex topography and dense forest canopies. Therefore, to increase confidence in our results and assess the impact of scale, we selected two ET products from different sensors using different algorithms. The first product we used was the MODIS (MOD16A2GF) Version 6 gap-filled ET product from 2000 - 2019 with 8-day 500m resolution (Running et al. 2019). The MOD16 ET algorithm is based on the Penman-Monteith logic (Monteith, 1965) and uses daily meteorological reanalysis data with MODIS vegetation indices, albedo, and land cover to calculate the sum of ET over each 8-day composite period (Running et al. 2019). The gap-filled product was chosen because cloud-contaminated leaf area index and fraction photosynthetically active radiation gaps were temporally filled using linear interpolation before calculating ET, mitigating the need to perform further quality control on the dataset. The second product we used was the Landsat Provisional Actual Evapotranspiration product from the U.S. Geological Survey (USGS), available every 8 to 16 days at 30m resolution from Landsat 4, 5, 7, and 8. This product is based on the Operational Simplified Surface Energy Balance (SSEBop) model (Senay, Gabriel B. et al., 2013; Senay, Gabriel B., 2018), which is a unique parameterization of the Simplified Surface Energy Balance model (SSEB) intended for operations applications (Senay, G. B., Budde, & Verdin, 2011; Senay, Gabriel B., Budde, Verdin, & Melesse, 2007). The algorithm combines ET fractions from soil and vegetation using Landsat Collection 1 Provisional Surface Temperature with reference ET based on the principle of satellite psychrometry, which assigns pre-defined seasonally dynamic boundary conditions to each pixel. All scenes intersecting the study area with less than 90% cloud cover from 1984 - 2020 were included in the analysis and pixels flagged as less than high quality were screened. ET could not be estimated for 153 Landsat scenes during the growing season (3.16% of total growing season scenes) because SSEBop model parameterization failed due to insufficient pixels with an NDVI greater than 0.7, likely due to high cloud cover, and resulted in consistently missing data in some parts of the landscape (Sayler & Zanter, 2020). We used Landsat data starting in 1984 even though MODIS data only became available in 2000 because Landsat scenes often were missing data and the longer record offered more

opportunities to quantify ET. We don't expect this difference to have a large impact on the analysis since we largely focus on quantifying the overall ET response to water availability.

Given the temporal scale mismatch between the MODIS and Landsat ET products, monthly seasonally standardized z-score ET anomalies were computed to make the results directly comparable. MODIS ET anomalies represent the average monthly 8-day ET rate (mm/8-day) and Landsat ET anomalies represent the average monthly ET rate (mm/day) and were calculated following:

$$Z_{i,j} = \frac{ET_{i,j} - \overline{ET}_i}{SD_i}$$

Where $Z_{i,j}$ is the seasonally z-score standardized anomaly for a given month and year where i is the month and j is the year, $ET_{i,j}$ is the average monthly ET rate, $\overline{ET}_i$ is the long term average ET rate for a given month, and SD_i is the long term standard deviation of the ET rate for a given month. The MODIS long term average and standard deviation calculations span 2000 - 2019 while the Landsat long term average and standard deviation calculations span 1984 - 2020.

2.3.2 ET Validation

Eddy covariance latent energy data from the USDA Forest Service Coweeta Hydrologic Laboratory flux tower were available from 2011-2015 and used to validate remotely sensed ET estimates (Oishi, A. C., 2020). Coweeta is located in western NC in the southern Appalachian Mountains (https://ameriflux.lbl.gov /sites/siteinfo/US-Cwt). Our comparisons included the ET rate at the original temporal resolution (MODIS: 8 day total; Landsat: daily overpass rate) and averaged by month (MODIS: average monthly 8-day total; Landsat: average monthly daily overpass). We calculated both MODIS and Landsat ET averages across a 300m radius tower footprint for the comparisons (Fisher et al., 2020). Since the tower is located in complex terrain that causes the footprint size and shape to vary (Novick, K., Brantley, Miniat, Walker, & Vose, 2014), we tested tower footprint sizes up to a 500m radius and found the performance metrics were not sensitive to radius size. We compared the remotely sensed ET to flux tower estimates using root mean square error (RMSE), mean average error (MAE), relative error (RE) calculated as MAE divided by average observed ET, as well as the slope and r-squared of a linear model.

2.4 Drought Index

The standardized precipitation index (SPI) is a measure of water availability based on the probability of receiving precipitation relative to the climatological average over a given temporal aggregation period (1 - 36 months) (Guttman, 1999). Since the index is based on a standardized probability, a value of -2 corresponds to precipitation aggregated over the chosen time scale that is two standard deviations below the climatological average for that time of year. We applied three-month SPI (SPI-3) because it has been shown to correspond closely with soil moisture drought (Nicolai-Shaw, Zscheischler, Hirschi, Gudmundsson, & Seneviratne, 2017; Wang, Rogers, & Munroe, 2015). Gridded SPI-3, available through

Google Earth Engine, was calculated from 4km daily Gridded Surface Meteorological (GRIDMET) datasets (Abatzoglou, 2013). To match the monthly ET anomalies, SPI-3 was averaged to a monthly time step and resampled to MODIS and Landsat spatial resolution.

2.5. Analyses of ET Drought Sensitivity

The ET analyses in the following sections were applied to both the Landsat and MODIS scale ET products.

2.5.1 Drought peak

According to the GRIDMET drought indices, a moderate drought corresponds to SPI values ranging from [-1.3 : -1.6), a severe drought corresponds to SPI values ranging from [-1.6 : -2.0), and an extreme drought corresponds to SPI values less than or equal to -2.0. We assigned the growing season month with the most negative SPI-3 that was less than or equal to -1.3 (moderate drought) as the drought peak. The gridded SPI-3 is standardized on a pixel basis, relative to the average precipitation received for a given time of year, which allows us to compare drought severity across precipitation gradients found along elevation and latitudinal gradients. We searched each pixel each year to identify any SPI-3 metrics that met the drought criteria, and for each drought event, we analyzed the drought peak. For all drought peaks, the average pixel-level ET anomaly (ET_{dp}) was calculated for all droughts and separately for each drought severity category. Additionally, the average pixel-level ET anomaly was calculated for normal wetness conditions (-0.5 > SPI-3 < 0.5) to serve as a comparison to the ET anomalies at drought peak.

2.5.2 Correlation of ET and SPI

To understand the relationship between ET and water availability, we calculated the spearman rank correlation coefficient between growing season monthly ET anomalies and monthly SPI for the full study period (R_{SPI-ET}). A positive correlation means ET increases with water availability, and the higher the correlation, the more sensitive ET is to dry periods and droughts. A negative correlation means ET decreases with increasing water availability, which is typically due reduced temperature and solar radiation associated with high levels of precipitation (Jiao et al., 2021). A lack of correlation implies ET is not responsive to water availability. To understand how R_{SPI-ET} has changed, we calculated 5-year rolling correlations for all windows with at least 50% of observations. The trend in the strength of the correlation over time (dR_{SPI-ET}) was calculated using Sen's slope and the Mann Kendall trend test (alpha <= 0.05) for pixels in which at least 25% of rolling correlation time steps were calculated. A significant, decreasing correlation magnitude means forest water use is becoming decoupled from water availability while a significant, increasing correlation magnitude suggests forest water use is becoming more sensitive to water availability.

2.5.3 ET response to water availability across environmental gradients

We assessed ET responses across elevation, hillslope, and percent diffuse-porous BA gradients to quantify the influence of topography and forest composition on ET response to water availability. We analyzed trends in ET_{dp}, R_{SPI-ET} and dR_{SPI-ET} across gradients of elevation, TWI, and percent diffuse-porous BA. The mean and standard deviation of ET_{dp}, R_{SPI-ET} and dR_{SPI-ET} was calculated at 50m elevation bins, 0.5 TWI bins (unitless), and 5% diffuse-porous BA bins. Binned ET_{dp} was further subset by drought severity categories. Bins with less than 100 pixels were excluded from the analysis. Trends in binned ET_{dp}, R_{SPI-ET} and dR_{SPI-ET} across environmental gradients were calculated using Sen's slope and Mann Kendall trend test (alpha <= 0.05) to analyze if there were significant changes across those gradients. We compared the MODIS and Landsat results to assess their robustness and assess differences resulting from the two RS based ET algorithms and scales. The pairwise Pearson correlation coefficient was calculated for elevation, TWI, and the percent diffuse-porous BA at MODIS and Landsat scale to further contextualize these results.

3. Results

3.1 Topographic Gradients

Forested area was distributed unevenly across elevation and hillslope gradients. The distribution of forest area by elevation bin is similar between MODIS and Landsat scale elevation, with the majority of forested area located between 500 - 1000m. Higher elevation forested areas (elevation > 1000m) accounted for an average between MODIS and Landsat of 22% of total forested area. Lower elevation forested areas (elevation < 500m) accounted for an average between MODIS and Landsat of 17.3% of total forested area. The distribution of forested area across TWI gradients varied more between MODIS and Landsat resolution but they are both skewed with long tails towards higher TWI values. At MODIS resolution, 27.3% of forested area was distributed over the lowest TWI values from 8 - 9, 64.7% of forested area distributed form 9 - 10, and 7.9% of forested area distributed across the highest TWI values from 10 - 20. At Landsat resolution, 17.7% of forested area was distributed over the lowest TWI values from 5.5 - 8, 60% of forested area distributed from 8 - 10, and the remaining 22.2% of forested area distributed over TWI values ranging 10 - 31.5.

3.2 RS based ET

We validated the RS ET estimates using eddy covariance flux tower ET. The MODIS ET (mm/8-day) product performed well with a RE of 28.375%, a slope of 0.98 and an R^2 of 0.82 (Table 1). Averaging the MODIS ET by month improved performance with a RE of 24.29%, a slope of 1.01 and an R^2 of 0.89 (Table 1). In comparison, Landsat ET (mm/day) did not perform as well as the MODIS ET. While the RE was comparable (RE = 29.02%), the slope (0.32) and the R^2 (0.41) were well below 1, indicating the Landsat ET was biased and underestimated ET (Table 1). Averaged by month, RE did not improve (31.42%) but slope (0.36) and R^2 (0.55) did improve (Table 1).

Table 1
Statistical metrics comparing flux tower ET and remote sensing based ET.

	N	RMSE	MAE	RE (%)	R^2	Slope
MODIS (8-day)	220	5.87	4.41	28.38	0.82	0.98
MODIS (monthly)	60	4.79	3.75	24.29	0.89	1.01
Landsat (daily)	61	1.16	0.88	29.02	0.41	0.32
Landsat (monthly)	29	1.19	0.9	31.42	0.55	0.36

3.3 Drought index

We used growing season SPI-3 to assess spatial patterns of drought severity and as an overall measure of water availability. SPI-3 was averaged across the study area to observe overall temporal trends in water availability from 1984 - 2020 (Fig. 2). Drier than average conditions (SPI-3 <= -1) and moderate drought (SPI-3 <= -1.3) occur frequently, while extreme droughts were uncommon in the Blue Ridge ecoregion. The two most extreme growing season droughts occurred in 1986 and 2007. Due to spatial averaging, Fig. 2 does not represent the full spectrum of drought experienced across the landscape. Drought severity varied across spatial gradients with a decrease in drought severity at the northern end of our study region.

3.4 Analyses of ET Drought Sensitivity

3.4.1 Drought peaks

We mapped ET_{dp} for all, moderate, severe, and extreme droughts using MODIS and Landsat ET (Fig. 3). The distribution of positive and negative ET_{dp} followed a distinct spatial pattern and varied between the MODIS and Landsat maps (Fig. 3). As drought severity increased, there were some gaps in the ETdp values because not all parts of the landscape experienced severe or extreme drought. The percent of positive ET_{dp} decreased with drought severity for MODIS while it increased for Landsat (Fig. 4). Across both sensors and for all levels of drought severity, at least 20% of impacted pixels had a positive ET_{dp} indicating higher ET during drought (Fig. 4).

3.4.2 Correlation of ET and SPI analysis

We identified a larger percentage of forested area where ET-water availability relationships were significant in the MODIS data compared to Landsat, with R_{SPI-ET} equal to 46.18% and 16.06% and dR_{SPI-ET} equal to 13.22% and 1.17% for MODIS and Landsat, respectively. The majority of forested pixels with a significant R_{SPI-ET} were positive and the majority of forested pixels with a significant dR_{SPI-ET} were negative for MODIS and Landsat.

3.4.3 ET response to water availability across environmental gradients

Pairwise Pearson correlation between elevation, TWI, and percent diffuse-porous BA revealed all three variables were significantly correlated at both the MODIS and Landsat scales, although MODIS correlations were stronger for all pairs (Table 2). MODIS elevation and percent diffuse-porous BA had the strongest correlation (0.60) while TWI and percent diffuse-porous had the weakest correlation (-0.17). At Landsat scale, elevation and percent diffuse-porous BA had the strongest correlation (0.39) and TWI and percent diffuse-porous BA had the lowest correlation (0.007) (Table 2).

Table 2
Pearson correlation between elevation, height above the nearest drainage, and the percent diffuse-porous BA for MODIS and Landsat resolution

MODIS	TWI	% diffuse-porous BA
Elevation	-0.34	0.6
TWI	1	-0.17
Landsat	TWI	% diffuse-porous BA
Elevation	-0.15	0.39
TWI	1	0.007

Sen's slope of binned ET_{dp} for all drought severity levels was positive across elevation gradients and negative across TWI gradients in both MODIS and Landsat, indicating ET_{dp} becomes less negative at higher elevations and drier, upslope positions (Fig. 5a-d). ET_{dp} was more negative as drought severity increased for MODIS ET but not Landsat ET (Fig. 4, 5). For MODIS ET, only the lowest elevation (< 600m) pixels had reduced water use during moderate drought, and even during extreme drought, over 1200m elevation ET_{dp} was comparable to that of no drought (Fig. 5a). In contrast, above 750m elevation, the binned Landsat ET_{dp} was greater than the no-drought average ET anomaly (Fig. 5b). We identified similar patterns along the TWI gradient, where only the wettest, most downslope MODIS pixels indicated a negative ET_{dp} during moderate drought; negative ET_{dp} only spread across the landscape at extreme drought levels (Fig. 5c). Similarly, Landsat indicated that only the pixels with the highest TWI values experience negative ET_{dp} regardless of drought severity (Fig. 5d). MODIS binned ET_{dp} showed increasingly divergent drought responses across the TWI and elevation gradients as drought severity increased (Fig. 5a-d). There were no significant trends in binned ET_{dp} over the percent diffuse-porous BA gradient for MODIS or Landsat (Fig. 5e-f).

While the significant MODIS R_{SPI-ET} was largely positive with a negative dR_{SPI-ET}, Landsat R_{SPI-ET} and dR_{SPI-ET} combinations varied across environmental gradients (Fig. 6). Despite the variability, both MODIS and Landsat ET indicated a decoupling between ET and SPI over time, especially at high elevations (Fig. 6). This means high elevation regions with a positive correlation tend to have negative trends and regions with a negative correlation tend to have positive trends, meaning those correlations are moving

closer to 0 over time (Fig. 6). R_{SPI-ET} decreased significantly with increasing elevation for MODIS and Landsat, however, these correlations diverged around 700m as Landsat R_{SPI-ET} became negative while MODIS R_{SPI-ET} remained positive (Fig. 6). Correlations also increased significantly with increasing TWI for both sensors but because of MODIS' coarser resolution it does not have data for TWI bins past 12 (Fig. 6). R_{SPI-ET} for MODIS and Landsat decreased with increasing percent of diffuse-porous BA but the binned R_{SPI-ET} remains positive across the gradient (Fig. 6).

Landsat and MODIS data indicate dR_{SPI-ET} diverges across elevation and percent diffuse-porous gradients. Across the elevation gradient, MODIS and Landsat have similar dR_{SPI-ET} until approximately 750m, when MODIS dR_{SPI-ET} becomes significantly more negative while Landsat dR_{SPI-ET} becomes significantly more positive (Fig. 6). This elevation threshold corresponds to the point where Landsat R_{SPI-ET} becomes negative while MODIS R_{SPI-ET} remains positive (Fig. 6). This indicates that as elevation increases, correlations are changing faster over time, and at higher elevations both sensors indicate a decoupling between ET and SPI (Fig. 6). Interestingly, Landsat binned dR_{SPI-ET} shows a positive trend across the percent diffuse-porous BA gradient while MODIS dR_{SPI-ET} shows a negative trend (Fig. 6). Given both Landsat and MODIS R_{SPI-ET} are positive, on average, across the gradient of percent diffuse-porous BA, MODIS shows a faster decrease in water availability constraints on highly diffuse-porous forest ET over time (Fig. 6). While the trend in Landsat dR_{SPI-ET} is significant and positive, the average dR_{SPI-ET} across the percent diffuse-porous gradient hovers close to 0 so the trend is largely trivial (Fig. 6). Across the TWI gradient MODIS has a positive significant trend in dR_{SPI-ET}, providing evidence of a faster decoupling at more upslope positions on the landscape, while Landsat does not have a significant trend.

4. Discussion

Our study indicates that at regional scales, forest response to drought varies across topographically complex terrain, and the differences are greater with increasing drought severity (Fig. 5). We found that trees in high elevation and dry, upslope portions of the landscape maintained stable water use (ET) rates even during extreme drought, while ET was reduced at low elevation and wet, downslope portions of the landscape, indicating these areas as more drought sensitive. This is consistent with findings at finer scales in the southern Appalachians and clarifies a few discrepancies between studies. Hwang (2020) reported that at the catchment scale, downslope trees experienced lower growth and greater sap flow sensitivity to soil moisture deficits compared to upslope trees during dry years, despite having higher soil moisture. Hawthorne and Miniat (2018) found that at low elevations, plot-level soil moisture and daily transpiration rates were greater at plots downslope during drought, which indicated downslope was more buffered from drought impacts (Hawthorne & Miniat, 2018).

Downslope portions of the landscape tend to have higher soil moisture and thus are dominated by the higher water use, drought sensitive, diffuse-porous species. During drought, these species may have higher water use sensitivity to soil moisture deficits while maintaining higher daily transpiration rates compared to upslope plots, which can help explain seemingly contrasting results from Hwang (2021) and

Hawthrone (2018). As drought severity increased, it is likely the unchanged or slightly increased forest water use at high elevations and upslope positions reduced downslope subsidies and led to the increasingly negative average ET anomalies at low elevations and downslope positions. These high elevation forests with unchanged or slightly increased forest water use tend to be located above 1000m, an area that comprises 22% of total forested area across the ecoregion. This indicates the high elevation forests have the potential to exert a large influence on reductions in lateral flow and streamflow generation, which directly influences water availability in downstream reaches important to larger metropolitan areas. Observed increases in ET, particularly upslope and at high elevations, have led to a decrease in downslope water subsidy and streamflow over time (Caldwell et al., 2016). This likely contributes to greater drought vulnerability of the downslope and low elevation forests that depend on upslope water subsidy to maintain soil moisture levels to support high daily transpiration and productivity.

Our analysis of both MODIS and Landsat ET data identified widespread above-average forest water use at drought peak, even during extreme drought, which could be related to rising temperatures and supported by deep soil moisture storage in the typically wet region (Fig. 4). Increasing temperatures have been reported across the southern Appalachian mountains (including the Blue Ridge Ecoregion), with growing season temperatures increasing by 0.48°C per decade since the 1970s in western North Carolina (Hwang et al., 2018; Hwang et al., 2020). Warmer temperatures increase evaporative demand, forcing vegetation to increase water use to support vegetation health, which propagates precipitation deficits faster and stronger downstream (Orth & Destouni, 2018). In fact, multiple investigations across forested mountain regions have quantified above average forest water use and reduced runoff generation at higher elevations due to local allocation of precipitation to transpiration, resulting in greater ecological vulnerability at lower elevations, likely due to decreased downslope subsidy (Goulden, M. L. & Bales, 2019; Goulden, Michael L. & Bales, 2014; Mastrotheodoros et al., 2020). While there is a discrepancy in the extent of positive ET_{dp} between MODIS and Landsat estimates, the pattern is still prevalent across sensors and drought severity levels which increases our confidence in this result (Fig. 4). Above average ET during drought likely directly translates to less streamflow generation, and ultimately less water flowing downstream, which contributes to lower low flows, larger societal impacts and greater vulnerability of aquatic biodiversity.

The discrepancies we identified between some of the MODIS and Landsat ET data highlight the importance of considering scale in remote sensing investigations over topographic gradients. While the MODIS data indicated that ET is less correlated to water availability at higher elevations and upslope positions, our analysis of Landsat correlations indicated that at high elevations, ET is more negatively correlated to water surpluses, likely due to associated decreased temperatures. This discrepancy could be tied to differences in spatial resolution between sensors because there is considerably less topographic variation within a 30m pixel compared to a 500m pixel. This allows Landsat to more precisely identify high elevation portions of the landscape compared to MODIS and reveal trends otherwise obscured by spatial averaging. Other studies indicate that higher elevation forests in the southern Appalachians tend

to be more strongly energy limited, which supports Landsat observations of negative R_{SPI-ET} (Hwang et al., 2012; Hwang et al., 2014). Both Landsat and MODIS analyses identified low elevation regions as the most water constrained (Fig. 6), which supports our other findings that low elevation and downslope portions of the landscape are the most drought sensitive compared to higher elevations or upslope areas (Tai et al., 2020). Low elevation forests below 500m and downslope forests with TWI greater than 10 display the greatest drought sensitivity across sensors and account for 17% and 15%, respectively, of total forested area, underscoring the widespread vulnerability of vegetation due to decreases in lateral flow.

Despite divergent trends in dR_{SPI-ET} between MODIS and Landsat ET, trends across both sensors are converging towards a decoupling of ET and SPI over time, indicating that ET is becoming less correlated to water availability over time. These trends occurred at a faster rate at high elevations, upslope positions, and in areas of forests with a higher percent diffuse-porous BA (Fig. 6). The drivers of this decoupling remain uncertain, but temperature is likely an important factor. As temperatures rise, forests are less energy limited (negative correlations become less negative) (Hwang et al., 2018) and evaporative demand rises which causes forests to use more water independent of availability (positive correlations become less positive) (Teuling et al., 2013).

Increases in forest water use efficiency (WUE) could also account for the decoupling of ET and water availability over time. Observed increases in forest WUE show that under elevated CO_2 concentrations, forests are able to maintain productivity using less water, allowing them to become less coupled with water availability (Keenan et al., 2013), but changes in WUE at the local scale are less conclusive. Interestingly, a recent study identified an increasing water constraint on vegetation growth across the extra-tropical northern hemisphere over the past 30 years and found that water savings from increased CO_2 did not offset the increasing water constraint (Jiao et al., 2021). In a more water limited Rocky Mountain watershed, the water savings attributed to stomatal closure associated with elevated CO_2, were offset by increased lateral flow, largely ameliorating the benefit to local vegetation (Tai, Venturas, Mackay, Brooks, & Flanagan, 2021). Coupled with changes in VPD, ET could increase and overwhelm the water saving effects of elevated CO_2 (Tai et al., 2021). Taken together, these findings suggest an increase in WUE is unlikely to explain our findings and indicates that WUE might decline if ET is maintained while vegetation growth is constrained.

We included forest composition as a potentially important explanatory variable in ET drought responses. We would expect forests with a greater percentage of diffuse-porous BA to be more tightly coupled with water availability because they have been shown to be more sensitive to soil moisture deficits than ring-porous species (Elliott et al., 2015; Meinzer et al., 2013). We found R_{SPI-ET} significantly decreased across the gradient in percent diffuse-porous BA and that over time ET has decoupled from water availability more quickly in forested areas with greater percent diffuse-porous BA (Fig. 6). While these trends are likely partially attributable to covariance of percent diffuse-porous BA with elevation and TWI (Table 2), it highlights that water use by forests composed of generally climate sensitive and high water use species

is becoming less constrained by water availability over time. It is possible that because extreme water stress is less common in the southern Appalachians, this reflects a decrease in sensitivity to water availability due to an increase in sensitivity to temperature or atmospheric demand. Novick (2016) found that climate change increases the role of VPD constraining water fluxes in eastern mesic forests, which could contribute to the decrease in coupling between ET and water availability. This means that high water use forests could maintain transpiration rates to satisfy atmospheric drought, which depletes soil moisture faster and leads to less runoff. Further, ongoing mesophication could exacerbate this feedback and we could see less runoff generation and more ecological stress as diffuse-porous species expand and forests maintain or increase ET at the expense of downslope subsidies.

It is important to consider the influence of the uncertainty associated with RS based ET estimates on our findings. We found that MODIS ET was more skilled at capturing ET variability than Landsat ET (Fig. 2). Estimates aggregated over longer periods of time tend to be more accurate, so the MODIS ET summed over 8-day periods was able to capture flux tower ET variability better than the Landsat daily overpass estimates. It is possible that the MODIS ET and Landsat ET performance would have been more comparable if we chose to aggregate ET to monthly totals. However, attempts at temporally interpolating Landsat ET between overpass dates to find monthly totals would likely be hindered by the frequent cloud cover characteristic of the southern Appalachians and produce estimates with similarly high uncertainty. To reduce algorithm complexity, monthly climatology reference ET is used in SSEBop as an auxiliary product to calculate actual ET which can lead to larger deviations from flux tower estimates on a given day compared to longer aggregations (Sayler & Zanter, 2020). In addition, a blocky artifact is noticeable in the Landsat ET estimates at high elevations due to coarse spatial resolution of the reference ET data used in elevated areas (Sayler & Zanter, 2020). Despite these drawbacks, SSEBop is still expected to adequately capture the spatial variability and all calculations were based on pixel-wise seasonally standardized average monthly anomalies, which should largely mitigate the above uncertainties.

5. Conclusion

Our study highlights a divergence in forest ET responses to drought over topographic gradients, despite large discrepancies between Landsat and MODIS ET results. We found high elevation and upslope regions maintain ET rates even during extreme droughts and have become less constrained by water availability over time. These regions account for a large proportion of forested area across the ecoregion, and coupled with the expansion of diffuse-porous trees across eastern forests, contribute to widespread decreases in lateral flow and greater vulnerability of downslope vegetation, streamflow, and aquatic biodiversity. Leveraging long-term remote sensing ET datasets allowed us to clarify topography-vegetation-drought sensitivity relationships at regional scales to understand systematic shifts in forest water cycling. Reliable remotely sensed ET in forested mountains is important to continue monitoring forest water use responses to hydroclimate variability and provides the necessary scope to assess global responses. Divergent forest water use responses between upslope vs downslope and high and low elevation regions should be further explored to understand how this could be exacerbated with continued global change.

Declarations

Acknowledgments

Funding

Conflicts of interest/Competing interest

Authors report no conflict of interest.

Ethics approval

Not applicable.

Consent to participate (include appropriate statements)

Not applicable.

Consent for publication (include appropriate statements)

All co-authors have approved the manuscript and agree with its submission to Landscape Ecology.

Availability of data and material (data transparency)

All data used in this study was publicly available online. Eddy covariance data was downloaded from Ameriflux (https://ameriflux.lbl.gov/sites/siteinfo/US-Cwt). GRIDMET SPI data, land cover data, and USGS NED data was downloaded from Google Earth Engine (https://earthengine.google.com/). MODIS ET data was downloaded from USGS (https://lpdaac.usgs.gov/products/mod16a2gfv006/). Landsat ET data was downloaded from USGS (https://www.usgs.gov/core-science-systems/nli/landsat/landsat-provisional-actual-evapotranspiration). The Riley (2021) forest composition map was downloaded from the USDA Forest Service (https://www.fs.usda.gov/rds/archive/Catalog/RDS-2019-0026). The Wilson (2013) forest composition maps were downloaded from the USDA forest service (https://www.fs.usda.gov/rds/archive/catalog/RDS-2013-0013).

Code availability (software application or custom code)

R scripts used for analysis and visualization are available on request.

Author's Contributions

K. McQuillan: Conceptualization, methodology, formal analysis, writing – original draft

M. Tulbure: Methodology, revisions

K. Martin: Conceptualization, methodology, writing and revisions

References

1. A. Christopher Oishi (2020), AmeriFlux BASE US-Cwt Coweeta, Ver. 1-5, AmeriFlux AMP, (Dataset). https://doi.org/10.17190/AMF/1671890

2. Abatzoglou, J. T. (2013). Development of gridded surface meteorological data for ecological applications and modelling. *International Journal of Climatology, 33*(1), 121-131. doi:10.1002/joc.3413

3. Bales, R. C., Goulden, M. L., Hunsaker, C. T., Conklin, M. H., Hartsough, P. C., O'Geen, A. T., . . . Safeeq, M. (2018). Mechanisms controlling the impact of multi-year drought on mountain hydrology. *Scientific Reports, 8* doi:10.1038/s41598-017-19007-0

4. Beven, K. J., & Kirkby, M. J. (1979). A physically based, variable contributing area model of basin hydrology / un modèle à base physique de zone d'appel variable de l'hydrologie du bassin versant. *Null, 24*(1), 43-69. doi:10.1080/02626667909491834

5. Caldwell, P. V., Miniat, C. F., Elliott, K. J., Swank, W. T., Brantley, S. T., & Laseter, S. H. (2016). Declining water yield from forested mountain watersheds in response to climate change and forest mesophication. *Global Change Biology, 22*(9), 2997-3012. doi:10.1111/gcb.13309

6. Elliott, K. J., Miniat, C. F., Pederson, N., & Laseter, S. H. (2015). Forest tree growth response to hydroclimate variability in the southern appalachians. *Global Change Biology, 21*(12), 4627-4641. doi:https://doi.org/10.1111/gcb.13045

7. Elliott, K. J., & Swank, W. T. (2008). Long-term changes in forest composition and diversity following early logging (1919–1923) and the decline of american chestnut (castanea dentata). *Plant Ecology, 197*(2), 155-172. doi:10.1007/s11258-007-9352-3

8. Falkenmark, M., & Rockström, J. (2006). The new blue and green water paradigm: Breaking new ground for water resources planning and management. *Journal of Water Resources Planning and Management, 132*(3), 129-132. doi:10.1061/(ASCE)0733-9496(2006)132:3(129)

9. Fan, Y., Clark, M., Lawrence, D. M., Swenson, S., Band, L. E., Brantley, S. L., . . . Yamazaki, D. (2019). Hillslope hydrology in global change research and earth system modeling. *Water Resources Research, 55*(2), 1737-1772. doi:10.1029/2018WR023903

10. Fisher, J. B., Lee, B., Purdy, A. J., Halverson, G. H., Dohlen, M. B., Cawse-Nicholson, K., . . . Hook, S. (2020). ECOSTRESS: NASA's next generation mission to measure evapotranspiration from the international space station. *Water Resources Research, 56*(4), e2019WR026058. doi:10.1029/2019WR026058

11. Fisher, J. B., Melton, F., Middleton, E., Hain, C., Anderson, M., Allen, R., . . . Wood, E. F. (2017). The future of evapotranspiration: Global requirements for ecosystem functioning, carbon and climate feedbacks, agricultural management, and water resources. *Water Resources Research, 53*(4), 2618-2626. doi:10.1002/2016WR020175

12. Ford, C. R., Hubbard, R. M., & Vose, J. M. (2011). Quantifying structural and physiological controls on variation in canopy transpiration among planted pine and hardwood species in the southern appalachians. *Ecohydrology, 4*(2), 183-195. doi:10.1002/eco.136

13. Friedl, M., Sulla-Menashe, D. (2019). *MCD12Q1 MODIS/Terra+Aqua Land Cover Type Yearly L3 Global 500m SIN Grid V006* [Data set]. NASA EOSDIS Land Processes DAAC. Accessed 2021-10-27 from https://doi.org/10.5067/MODIS/MCD12Q1.006

14. Gesch, D. B., Evans, G. A., Oimoen, M. J., & Arundel, S. (2018). The national elevation dataset. (pp. 83-110) American Society for Photogrammetry and Remote Sensing. Retrieved from http://pubs.er.usgs.gov/publication/70201572

15. Goulden, M. L., & Bales, R. C. (2019). California forest die-off linked to multi-year deep soil drying in 2012–2015 drought. *Nature Geoscience, 12*(8), 632-637. doi:10.1038/s41561-019-0388-5

16. Goulden, M. L., & Bales, R. C. (2014). Mountain runoff vulnerability to increased evapotranspiration with vegetation expansion. *Proceedings of the National Academy of Sciences, 111*(39), 14071-14075.

17. Guttman, N. B. (1999). Accepting the standardized precipitation index: A calculation Algorithm1. *JAWRA Journal of the American Water Resources Association, 35*(2), 311-322. doi:10.1111/j.1752-1688.1999.tb03592.x

18. Hawthorne, S., & Miniat, C. F. (2018). Topography may mitigate drought effects on vegetation along a hillslope gradient. *Ecohydrology, 11*(1), e1825. doi:https://doi.org/10.1002/eco.1825

19. Hoylman, Z. H., Jencso, K. G., Hu, J., Martin, J. T., Holden, Z. A., Seielstad, C. A., & Rowell, E. M. (2018). Hillslope topography mediates spatial patterns of ecosystem sensitivity to climate. *Journal of Geophysical Research: Biogeosciences, 123*(2), 353-371. doi:10.1002/2017JG004108

20. Hwang, T., Band, L. E., Miniat, C. F., Song, C., Bolstad, P. V., Vose, J. M., & Love, J. P. (2014). Divergent phenological response to hydroclimate variability in forested mountain watersheds. *Global Change Biology, 20*(8), 2580-2595. doi:10.1111/gcb.12556

21. Hwang, T., Band, L. E., Miniat, C. F., Vose, J. M., Knoepp, J. D., Song, C., & Bolstad, P. V. (2020). Climate change may increase the drought stress of mesophytic trees downslope with ongoing forest mesophication under a history of fire suppression. *Frontiers in Forests and Global Change, 3* doi:10.3389/ffgc.2020.00017

22. Hwang, T., Band, L. E., Vose, J. M., & Tague, C. (2012). Ecosystem processes at the watershed scale: Hydrologic vegetation gradient as an indicator for lateral hydrologic connectivity of headwater catchments. *Water Resources Research, 48*(6) doi:10.1029/2011WR011301

23. Hwang, T., Martin, K. L., Vose, J. M., Wear, D., Miles, B., Kim, Y., & Band, L. E. (2018). Nonstationary hydrologic behavior in forested watersheds is mediated by climate-induced changes in growing

season length and subsequent vegetation growth. *Water Resources Research, 54*(8), 5359-5375. doi:10.1029/2017WR022279

24. Jiao, W., Wang, L., Smith, W. K., Chang, Q., Wang, H., & D'Odorico, P. (2021). Observed increasing water constraint on vegetation growth over the last three decades. *Nature Communications, 12*(1), 1-9. doi:10.1038/s41467-021-24016-9

25. Keenan, T. F., Hollinger, D. Y., Bohrer, G., Dragoni, D., Munger, J. W., Schmid, H. P., & Richardson, A. D. (2013). Increase in forest water-use efficiency as atmospheric carbon dioxide concentrations rise. *Nature, 499*(7458), 324-327. doi:10.1038/nature12291

26. Kelly, A. E., & Goulden, M. L. (2008). Rapid shifts in plant distribution with recent climate change. *Proc Natl Acad Sci USA, 105*(33), 11823. doi:10.1073/pnas.0802891105

27. Lin, L., Band, L. E., Vose, J. M., Hwang, T., Miniat, C. F., & Bolstad, P. V. (2019). Ecosystem processes at the watershed scale: Influence of flowpath patterns of canopy ecophysiology on emergent catchment water and carbon cycling. *Ecohydrology, 12*(5), e2093. doi:10.1002/eco.2093

28. McKay, L., Bondelid, T., Dewald, T., Johnston, J., Moore, R., and Rea, A., "NHDPlus Version 2: User Guide", 2012

29. Mastrotheodoros, T., Pappas, C., Molnar, P., Burlando, P., Manoli, G., Parajka, J., . . . Fatichi, S. (2020). More green and less blue water in the alps during warmer summers. *Nature Climate Change, 10*(2), 155-161. doi:10.1038/s41558-019-0676-5

30. Meinzer, F. C., Woodruff, D. R., Eissenstat, D. M., Lin, H. S., Adams, T. S., & McCulloh, K. A. (2013). Above- and belowground controls on water use by trees of different wood types in an eastern US deciduous forest. *Tree Physiology, 33*(4), 345-356. doi:10.1093/treephys/tpt012

31. Monteith, J. L. (1965). Evaporation and environment. *Symposia of the Society for Experimental Biology, 19*, 205-234.

32. Mu, Q., Heinsch, F. A., Zhao, M., & Running, S. W. (2007). Development of a global evapotranspiration algorithm based on MODIS and global meteorology data. *Remote Sensing of Environment, 111*(4), 519-536. doi:10.1016/j.rse.2007.04.015

33. Nicolai-Shaw, N., Zscheischler, J., Hirschi, M., Gudmundsson, L., & Seneviratne, S. I. (2017). A drought event composite analysis using satellite remote-sensing based soil moisture. *Remote Sensing of Environment, 203*, 216-225. doi:10.1016/j.rse.2017.06.014

34. Novick, K., Brantley, S., Miniat, C. F., Walker, J., & Vose, J. M. (2014). Inferring the contribution of advection to total ecosystem scalar fluxes over a tall forest in complex terrain. *Agricultural and Forest Meteorology, 185*, 1-13. doi:10.1016/j.agrformet.2013.10.010

35. Novick, K. A., Ficklin, D. L., Stoy, P. C., Williams, C. A., Bohrer, G., & et al. (2016). The increasing importance of atmospheric demand for ecosystem water and carbon fluxes - ProQuest. *Nature Climate Change1, 6*(11) Retrieved from https://search-proquest-com.prox.lib.ncsu.edu/docview/1833258797?pq-origsite=summon

36. Nowacki, G. J., & Abrams, M. D. (2008). The demise of fire and "Mesophication" of forests in the eastern united states. *BioScience, 58*(2), 123-138. doi:10.1641/B580207

37. Orth, R., & Destouni, G. (2018). Drought reduces blue-water fluxes more strongly than green-water fluxes in europe. *Nature Communications, 9*(1), 1-8. doi:10.1038/s41467-018-06013-7

38. Pascolini-Campbell, M., Reager, J. T., Chandanpurkar, H. A., & Rodell, M. (2021). A 10 per cent increase in global land evapotranspiration from 2003 to 2019. *Nature, 593*(7860), 543-547. doi:10.1038/s41586-021-03503-5

39. Pederson, N., D'Amato, A. W., Dyer, J. M., Foster, D. R., Goldblum, D., Hart, J. L., . . . Williams, J. W. (2015). Climate remains an important driver of post-european vegetation change in the eastern united states. *Global Change Biology, 21*(6), 2105-2110. doi:10.1111/gcb.12779

40. Pittillo, J. D., Hatcher, R. D., & Buol, S. W. (1998). Introduction to the environment and vegetation of the southern blue ridge province. *Castanea, 63*(3), 202-216. Retrieved from http://www.jstor.org/stable/4033976

41. Rangwala, I., & Miller, J. R. (2012). Climate change in mountains: A review of elevation-dependent warming and its possible causes. *Climatic Change, 114*(3), 527-547. doi:10.1007/s10584-012-0419-3

42. Riley, K. L., Grenfell, I. C., Finney, M. A., & Wiener, J. M. (2021). TreeMap, a tree-level model of conterminous US forests circa 2014 produced by imputation of FIA plot data. *Scientific Data, 8*(1), 1-14. doi:10.1038/s41597-020-00782-x

43. Running, S., Mu, Q., Zhao, M., Moreno, A. (2019). *MOD16A2GF MODIS/Terra Net Evapotranspiration Gap-Filled 8-Day L4 Global 500 m SIN Grid V006* [Data set]. NASA EOSDIS Land Processes DAAC. Accessed 2021-08-07 from https://doi.org/10.5067/MODIS/MOD16A2GF.006

44. Sayler, K., Zanter, K. (2020). Landsat Provisional Actual Evapotranspiration (ETa) Product Guide. U.S. Geological Survey

45. Senay, G. B., Budde, M. E., & Verdin, J. P. (2011). Enhancing the simplified surface energy balance (SSEB) approach for estimating landscape ET: Validation with the METRIC model. *Agricultural Water Management, 98*(4), 606-618. doi:10.1016/j.agwat.2010.10.014

46. Senay, G. B. (2018). Satellite psychrometric formulation of the operational simplified surface energy balance (SSEBop) model for quantifying and mapping evapotranspiration. *Applied Engineering in Agriculture, . 34*, pp. 555-2018 v.34 no.3; 566. doi:10.13031/aea.12614

47. Senay, G. B., Bohms, S., Singh, R. K., Gowda, P. H., Velpuri, N. M., Alemu, H., & Verdin, J. P. (2013). Operational evapotranspiration mapping using remote sensing and weather datasets: A new parameterization for the SSEB approach. *JAWRA Journal of the American Water Resources Association, 49*(3), 577-591. doi:10.1111/jawr.12057

48. Senay, G. B., Budde, M., Verdin, J. P., & Melesse, A. M. (2007). *A coupled remote sensing and simplified surface energy balance approach to estimate actual evapotranspiration from irrigated fields* doi:10.3390/s7060979

49. Senay, G. B., Schauer, M., Friedrichs, M., Velpuri, N. M., & Singh, R. K. (2017). Satellite-based water use dynamics using historical landsat data (1984–2014) in the southwestern united states. *Remote Sensing of Environment, 202*, 98-112. doi:10.1016/j.rse.2017.05.005

50. Tai, X., Anderegg, W. R. L., Blanken, P. D., Burns, S. P., Christensen, L., & Brooks, P. D. (2020). Hillslope hydrology influences the spatial and temporal patterns of remotely sensed ecosystem productivity. *Water Resources Research, 56*(11), e2020WR027630. doi:10.1029/2020WR027630

51. Tai, X., Venturas, M. D., Mackay, D. S., Brooks, P. D., & Flanagan, L. B. (2021). Lateral subsurface flow modulates forest mortality risk to future climate and elevated CO2. *Environmental Research Letters, 16*(8), 084015. doi:10.1088/1748-9326/ac1135

52. Teuling, A. J., Loon, A. F. V., Seneviratne, S. I., Lehner, I., Aubinet, M., Heinesch, B., . . . Spank, U. (2013). Evapotranspiration amplifies european summer drought. *Geophysical Research Letters, 40*(10), 2071-2075. doi:10.1002/grl.50495

53. Tromp-van Meerveld, H. J., & McDonnell, J. J. (2006). On the interrelations between topography, soil depth, soil moisture, transpiration rates and species distribution at the hillslope scale. *Advances in Water Resources, 29*(2), 293-310. doi:10.1016/j.advwatres.2005.02.016

54. Wang, H., Rogers, J. C., & Munroe, D. K. (2015). Commonly used drought indices as indicators of soil moisture in china. *Journal of Hydrometeorology, 16*(3), 1397-1408. doi:10.1175/JHM-D-14-0076.1

55. Wilson, Barry Tyler; Lister, Andrew J.; Riemann, Rachel I.; Griffith, Douglas M. 2013. Live tree species basal area of the contiguous United States (2000-2009). Newtown Square, PA: USDA Forest Service, Rocky Mountain Research Station. https://doi.org/10.2737/RDS-2013-0013

56. Yang, L., Jin, S., Danielson, P., Homer, C., Gass, L., Bender, S. M., . . . Xian, G. (2018). A new generation of the united states national land cover database: Requirements, research priorities, design, and implementation strategies. *ISPRS Journal of Photogrammetry and Remote Sensing, 146*, 108-123. doi:https://doi-org.prox.lib.ncsu.edu/10.1016/j.isprsjprs.2018.09.006

57. Yang, Y., Anderson, M. C., Gao, F., Hain, C. R., & semmens, K. A. (2015). Daily landsat-scale evapotranspiration estimation over a forested landscape in north carolina, USA, using multi-satellite data fusion. *Hydrology and Earth System Sciences, 21*(2), 1017-1037. Retrieved from https://search-proquest-com.prox.lib.ncsu.edu/docview/1868927281?pq-origsite=summon
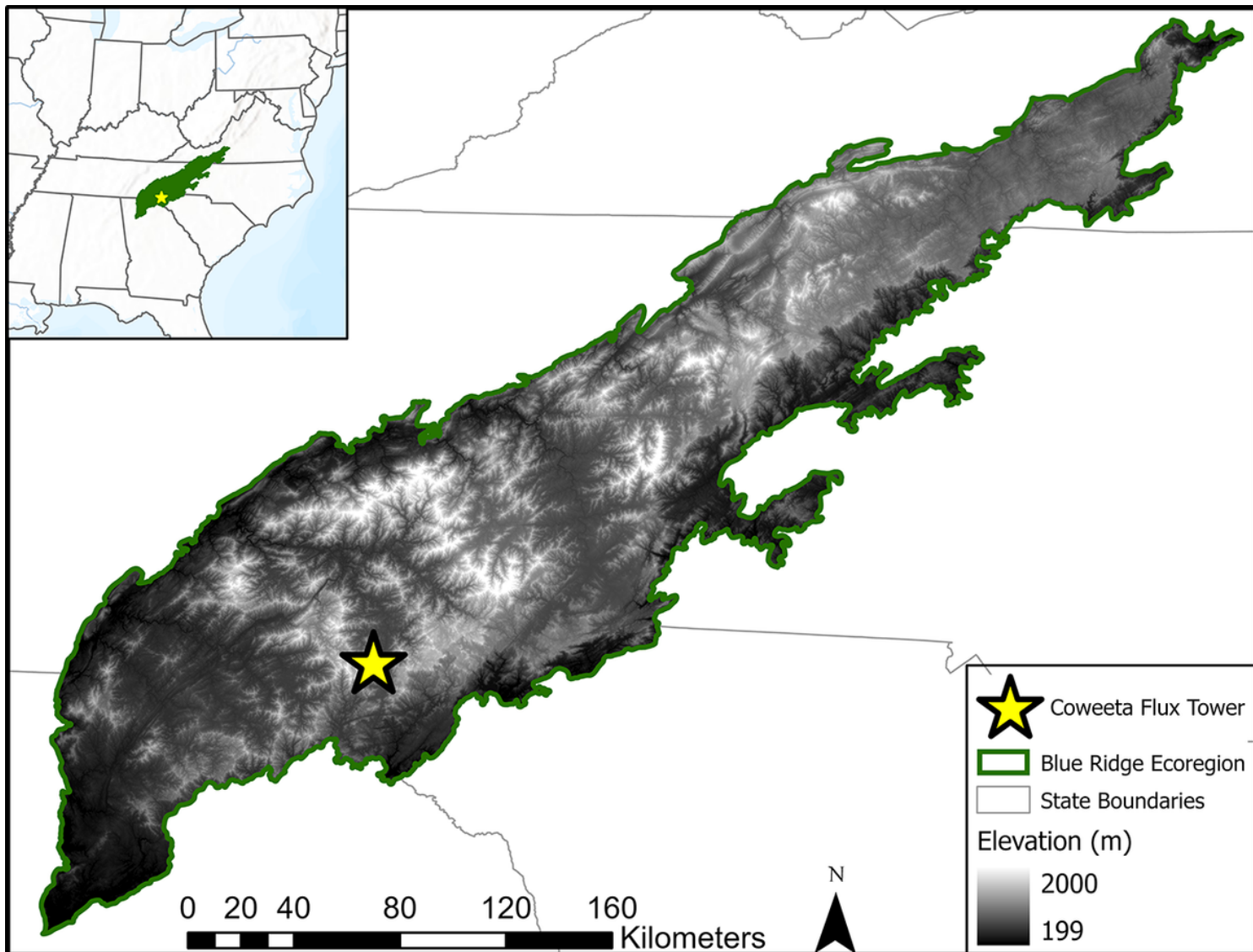
Figures

Figure 1

Map of the study area delineated by the Blue Ridge ecoregion and elevation (USGS NED). The yellow star represents the location of the Coweeta Hydrologic Laboratory eddy covariance flux tower used for RS based ET validation.
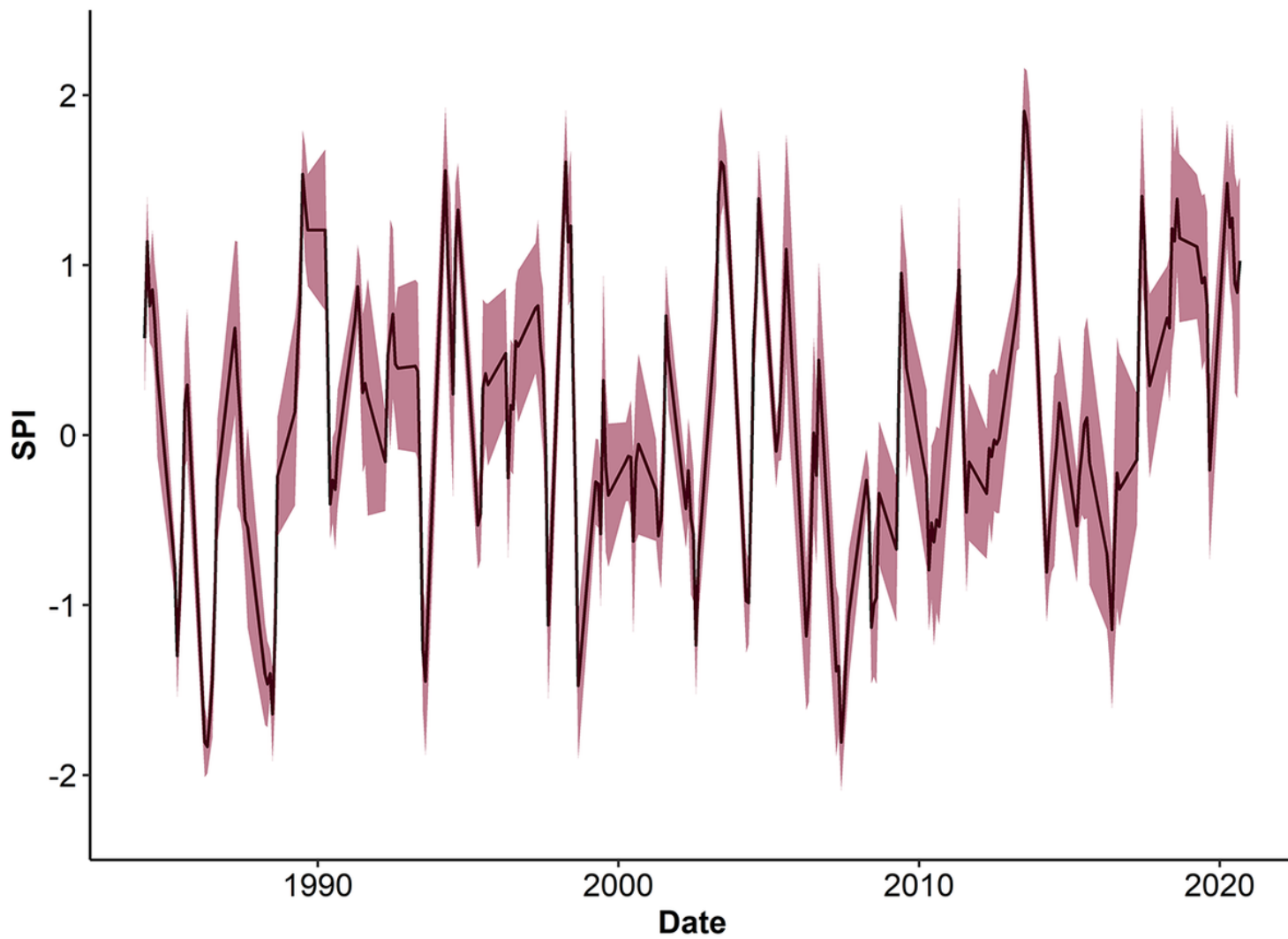
Figure 2

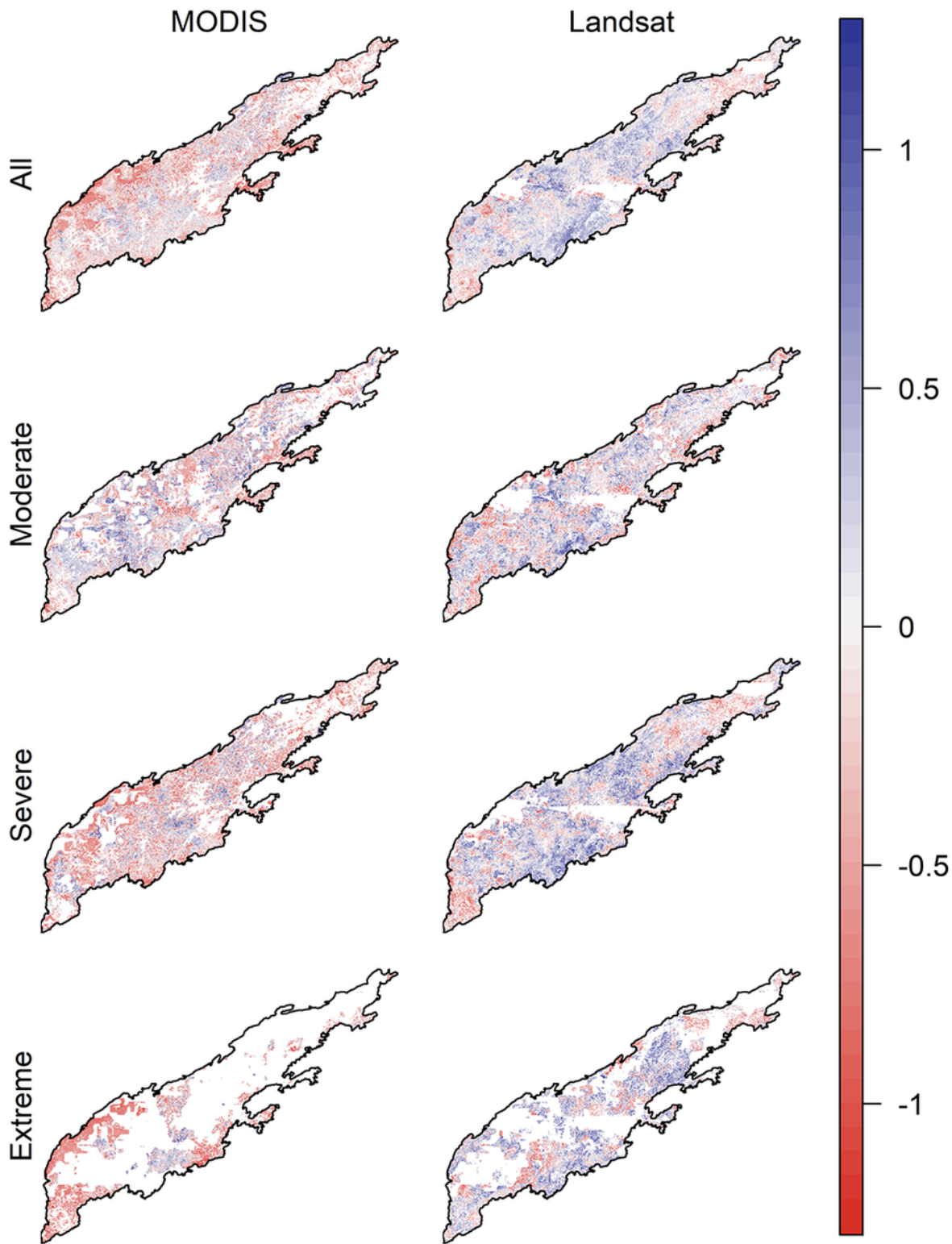Monthly SPI-3 from 1984 - 2020 averaged across the study area. The area shaded red is +/- 1 SD.

Figure 3

MODIS and Landsat ET anomalies averaged at drought peak (ETdp) for all (SPI <= -1.3), moderate (-1.6 < SPI <= -1.3), severe (-2.0 < SPI <= -1.6), and extreme droughts (SPI <= -2.0). Pixels with no data or that did not experience a drought at a given severity are in white.
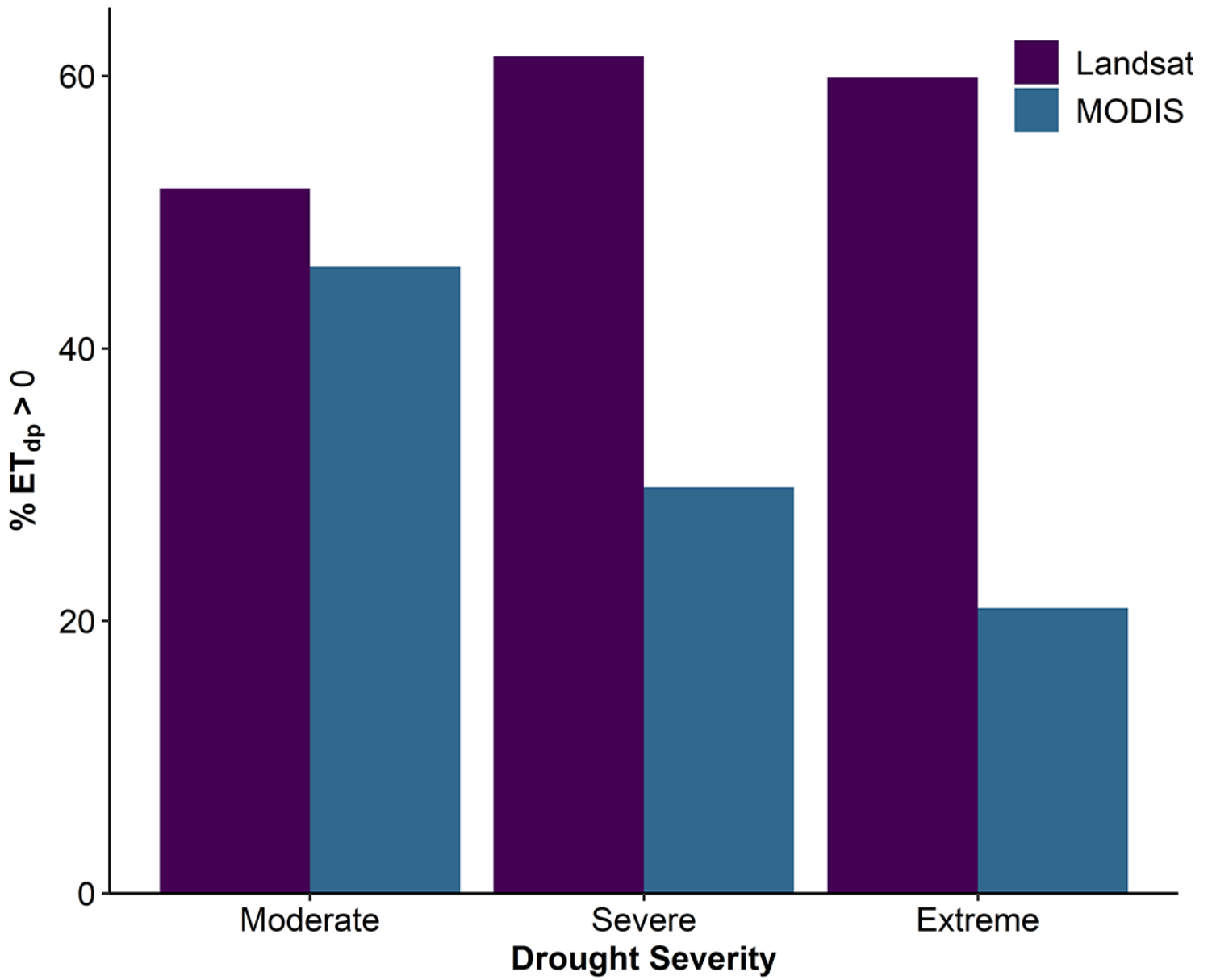
Figure 4

The percentage of averaged ET anomalies at drought peak (ETdp) that are greater than 0, indicating higher than expected water use, subset by drought severity for Landsat and MODIS.
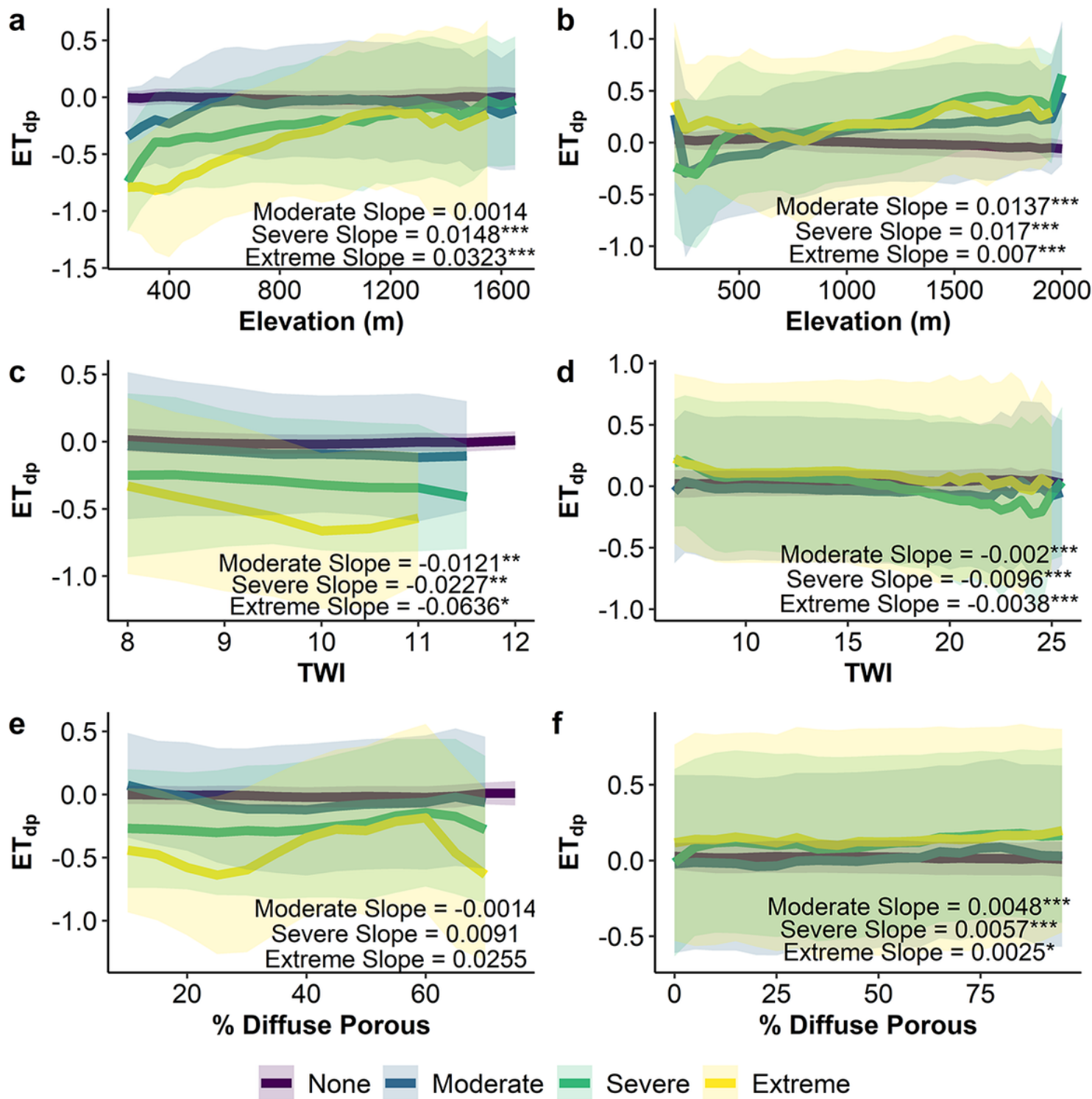
Figure 5

Binned ET anomalies at drought peak (ETdp) +/- 1 SD broken down by drought severity across elevation (a,b), TWI (c,d) and % diffuse-porous BA gradients (e,f) for MODIS (a,c,e) and Landsat (b,d,f). Sen's slope and Man Kendall test computed separately for MODIS and Landsat at each drought severity level to identify significant trends across gradients with significance denoted as * <= 0.05, ** <= 0.01, *** <= 0.001.
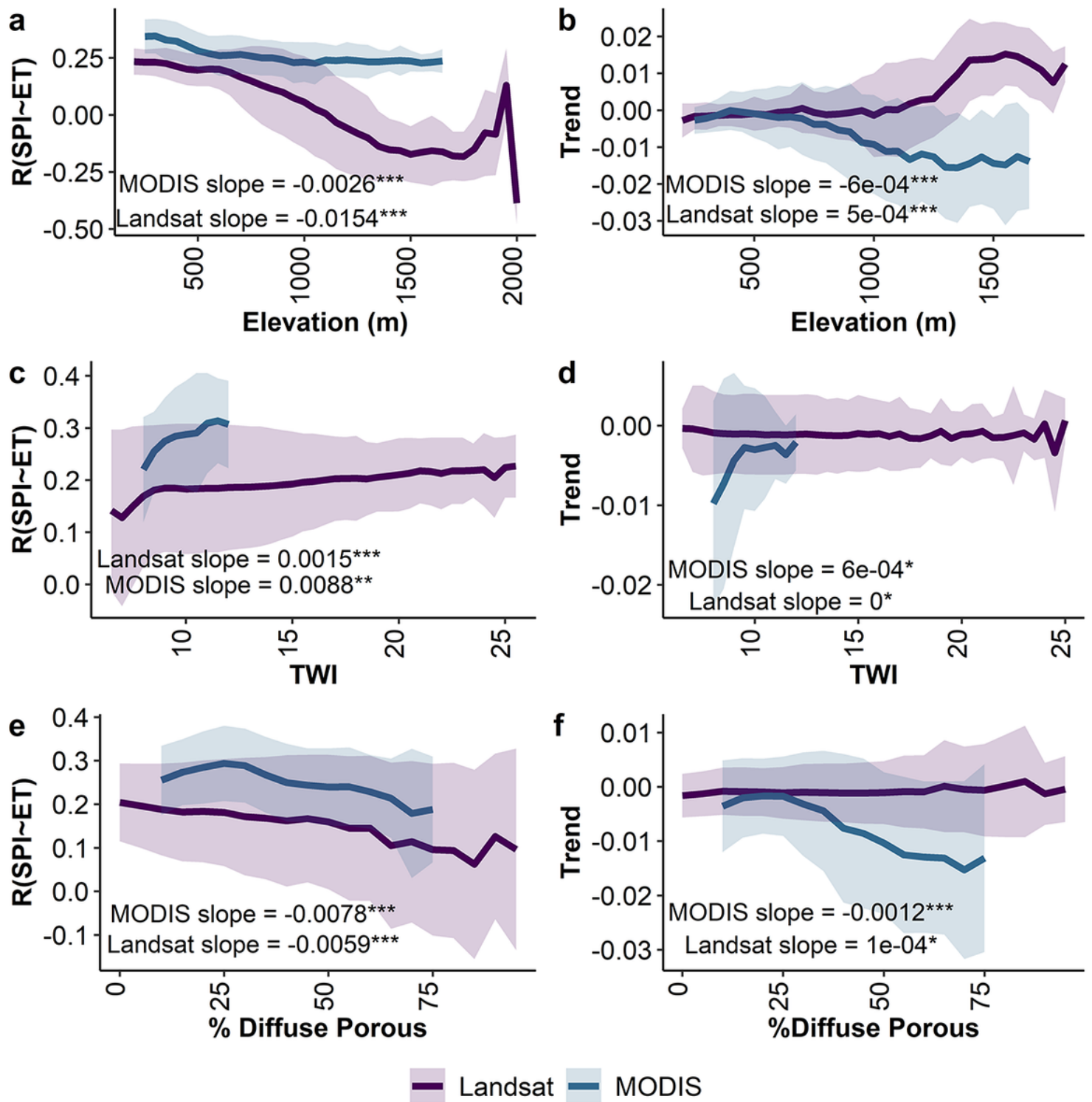
Figure 6

Binned overall correlation between ET and SPI (RSPI-ET) (a,c,e) and the trend in overall correlation (dRSPI-ET) (b,d,f) +/- 1 SD across elevation (a,b), TWI (c,d) and percent diffuse-porous BA (e,f) gradients for Landsat and MODIS. Sen's slope and Man Kendall test computed separately for MODIS and Landsat to identify significant trends across gradients with significance denoted as * <= 0.05, ** <= 0.01, *** <= 0.001.

Supplementary Files

This is a list of supplementary files associated with this preprint. Click to download.

- SupplementaryInformation.pdf